JACS
JOURNAL OF THE AMERICAN CHEMICAL SOCIETY

Article

pubs.acs.org/JACS

Revealing the Binding Structure of the Protein Corona on Gold Nanorods Using Synchrotron Radiation-Based Techniques: Understanding the Reduced Damage in Cell Membranes

Liming Wang,[†,‡] Jingyuan Li,[†,‡] Jun Pan,[†] Xiumei Jiang,[†] Yinglu Ji,[⊥] Yufeng Li,[†] Ying Qu,[†] Yuliang Zhao,[†] Xiaochun Wu,*[,⊥] and Chunying Chen*[,†]

[†]CAS Key Laboratory for Biomedical Effects of Nanomaterials and Nanosafety, National Center for Nanoscience and Technology of China and Institute of High Energy Physics, Beijing, China

[⊥]CAS Key Laboratory of Standardization and Measurement for Nanotechnology, National Center for Nanoscience and Technology of China, Beijing, China

Supporting Information

ABSTRACT: Regarding the importance of the biological effects of nanomaterials, there is still limited knowledge about the binding structure and stability of the protein corona on nanomaterials and the subsequent impacts. Here we designed a hard serum albumin protein corona (BSA) on CTAB-coated gold nanorods (AuNRs) and captured the structure of protein adsorption using synchrotron radiation X-ray absorption spectroscopy, microbeam X-ray fluorescent spectroscopy, and circular dichroism in combination with molecular dynamics simulations. The protein adsorption is attributed to at least 12 Au−S bonds and the stable corona reduced the cytotoxicity of CTAB/AuNRs. These combined strategies using physical, chemical, and biological approaches will improve our understanding of the protective effects of protein coronas against the toxicity of nanomaterials. These findings have shed light on a new strategy for studying interactions between proteins and nanomaterials, and this information will help further guide the rational design of nanomaterials for safe and effective biomedical applications.

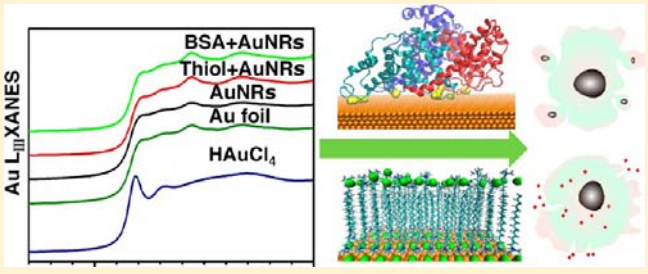

1. INTRODUCTION

When nanoparticles (NPs) enter the blood or other physiological fluids, various proteins can be easily adsorbed on the surface to reduce the free energy[1,2] and finally form protein coronas on a variety of common nanomaterials including gold,[3] silver,[4] carbon,[5,6] polystyrene,[7,8] silica,[9] and titania.[10] The binding tightness and stability of a surface protein corona define it as "hard" or "soft".[2] The protein corona affects various biological responses,[3−6,11−20] especially mitigated cytotoxicity,[5,6,12,15,18] changes in the biodistribution,[3,16,19] and inflammatory responses.[20] Recent research has shown that poly(acrylic acid)-conjugated gold nanoparticles (AuNPs) at a certain size can easily bind to and induce unfolding of fibrinogen, a plasma protein, and further promote the activation of Mac-1 receptor-dependent inflammation.[20] The protein corona on the AuNPs is also found to play an essential role in mediating cellular uptake[11,24] and cytotoxicity[25,26] as well as in realizing biomedical applications.[21,22] Moreover, corona−NP complexes can also be designed as drug carriers and imaging probes.[21,22] One successful example is that serum albumin may help drugs such as Abraxane (an FDA-approved drug in the form of albumin-bound paclitaxel) to achieve prolonged circulation time *in vivo*.[23] PEGylated transferrin (Tf) corona-conjugated silica NPs lose targeting specificity *in vivo* because the Tf corona can be exchanged for other proteins in the serum.[27] Improvement of the stability of the Tf corona on the NPs is thus crucial for their targeted applications *in vivo*. Therefore, knowledge of the binding characteristics of the protein corona to NPs would largely help address the underlying mechanism for its stability and potential biological impact, which should inspire further prediction of their *in vivo* fate and behavior.

However, little has been known about how the corona forms and the interfacial structures between corona and NPs. Recently, the binding of the corona to NPs has been explored with a variety of analytical techniques commonly used to characterize protein composition and species,[3,7,28] thickness,[12,19] binding affinity and stability,[9,27,29] and conformation of the protein corona.[30,31] The conformation and binding mode of proteins in the corona can be characterized by circular dichroism (CD), nuclear magnetic resonance (NMR), X-ray crystallography, and other techniques.[20,31−33] However, NMR and X-ray crystallography face the difficulties of complicated sample preparation, expense, and time-intensive measurements.[34] The NMR method is also not applicable to sulfur-

Received: July 8, 2013
Published: November 12, 2013

   dx.doi.org/10.1021/ja406924v | J. Am. Chem. Soc. 2013, 135, 17359−17368

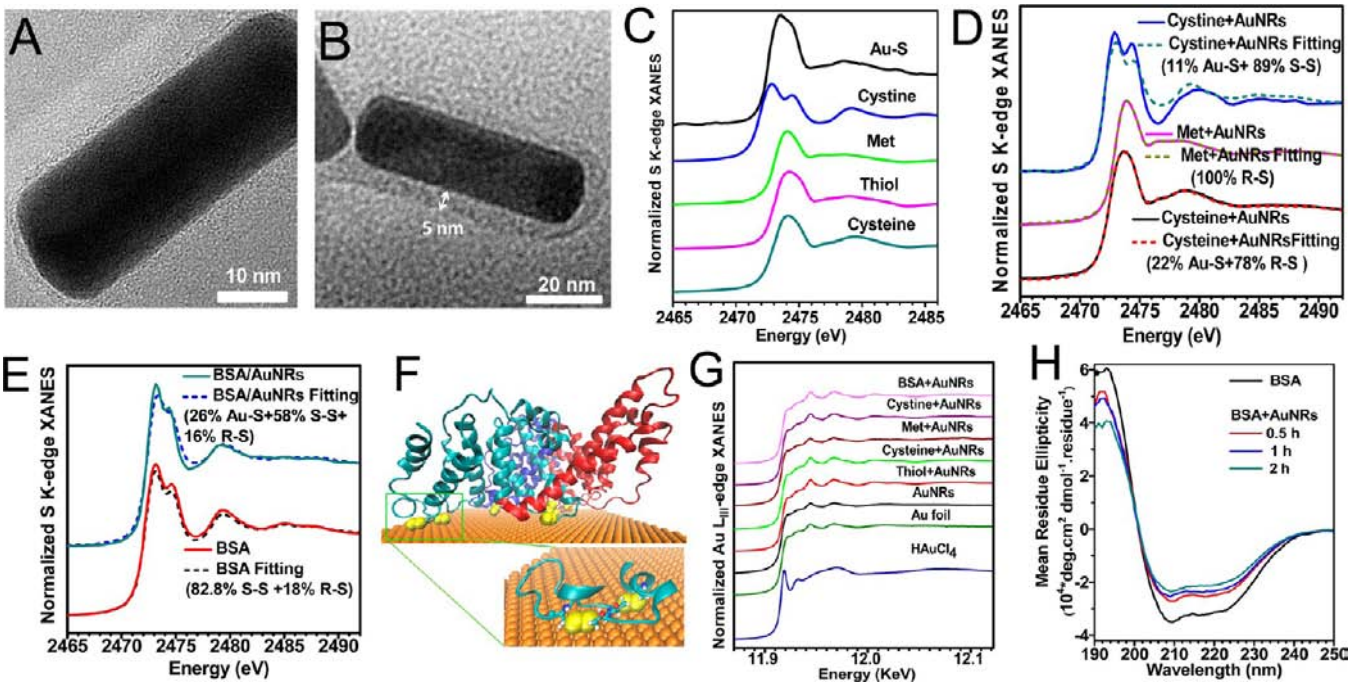

Figure 1. Interaction between AuNRs and sulfur-containing molecules (BSA, cysteine, cystine, methionine, and 11-mercaptoundecanoic acid (MUA, thiol)). Characterization of CTAB/AuNRs (A) and BSA corona-coated AuNRs (B) according to TEM imaging. (C) Various sulfur species in reference samples: Au−S, R−S (cysteine, thiol, Met), and R−S−S−R′ (cystine), shown as normalized S K-edge XANES spectra. (D) Chemical species of sulfur in cysteine, Met, and cystine after incubation with AuNRs. (E) Composite of sulfur chemical species in BSA and the BSA corona on AuNRs. (F) Disulfides of BSA (yellow) binding to the Au (111) surface of AuNRs. BSA is rendered as a cartoon representation with the three domains colored cyan, red, and blue. Inset: zoomed, two disulfide moieties colored yellow on the surface of Au from the green segment (G) Chemical species of gold in the reference samples (Au foil and $HAuCl_4$) and in other samples including AuNRs and AuNRs incubated with BSA, cysteine, cystine, and thiol, respectively. The chemical species of gold are shown as normalized gold L_{III} edge XANES. (H) Changes in the secondary structures of BSA adsorbed on AuNRs, determined by CD spectroscopy. In (D) and (E), normalized XANES spectra are presented as solid lines, and the least-squares fitting results as short dashed lines.

related structures due to the absence of nuclear spin or weak signals from ^{32}S and/or its isotopes.[35]

Unlike these conventional techniques, an advantage in studying the structures of nanomaterials and biological molecules is provided by synchrotron radiation (SR)-based analytical techniques.[36−40] A SR light source can provide very bright light with a tunable energy range and a high density of photons. SR X-ray absorption near-edge structures (XANES) can sensitively detect the composition of chemical species of sulfur[35,36,38,41] and thus present advantages in characterizing the interaction mode of the protein corona on AuNPs as either physical or chemical adsorption. Meanwhile, an SR-based microbeam X-ray fluorescence (μ-XRF) technique can simultaneously detect multiple elements, map their distribution, and semiquantify their concentrations in a tissue slice or even a single cell.[37,42−44] In the theoretical realm, molecular dynamics (MD) simulation has been widely used to study the interaction of proteins with NPs.[5,31,34] It can reveal the binding process of a protein, describe the preferred binding sites, and probe the concomitant conformational change of the adsorbed protein in detail. Therefore, it becomes a powerful approach to studying the binding mode and structure of protein corona on AuNPs at the atomic level when combined with analytical tools like XANES.

Gold nanorods in particular have wide applications in biomedicine[45−49] and their potential impacts on living systems are attracting much attention. Our recent study has revealed that serum protein (e.g., fetal bovine serum, FBS) corona on cetyltrimethylammonium bromide-capped gold nanorods (CTAB/AuNRs) can mitigate damage to the cell membrane before internalization and reduce the necrosis induced by CTAB/AuNRs.[50] Interestingly, after internalization and translocation into lysosomes, the protein corona can then be detached from the AuNRs, and finally the CTAB/AuNRs induce apotosis.[19] Similarly, a very recent study has indicated that this adsorbed protein corona is strong enough to be retained on the NPs as they enter the cell and are trafficked to the lysosomes. The corona would reduce the direct contact of the NPs with the cell membranes and protects the cells from the damages in the membrane caused by the toxic surface of NPs until it is enzymatically cleared in the lysosomes.[18] It is also possible that the conformational change in serum proteins induced by binding to AuNRs would result in dysfunction of the proteins. Thus, a detailed study of the binding stability of the protein corona on CTAB/AuNRs and their corresponding binding structure may be crucial to understanding such dynamic phenomena. Bovine serum albumin (BSA) is known as the most abundant representative serum protein. Knowledge of its adsorption on AuNRs is helpful for understanding the formation of FBS coronas in real situations and their role in reducing cytotoxicity.

In the present study, we selected BSA as a model protein, aiming to form a hard BSA corona around the AuNRs and further investigate the interaction mode of the BSA corona with AuNRs (e.g., binding interface, crucial residues, conformation of protein, etc.) by combining the experimental approaches of XANES and CD with MD simulation. The disulfide bonds in the BSA corona were found to directly recognize the gold

dx.doi.org/10.1021/ja406924v | J. Am. Chem. Soc. 2013, 135, 17359−17368

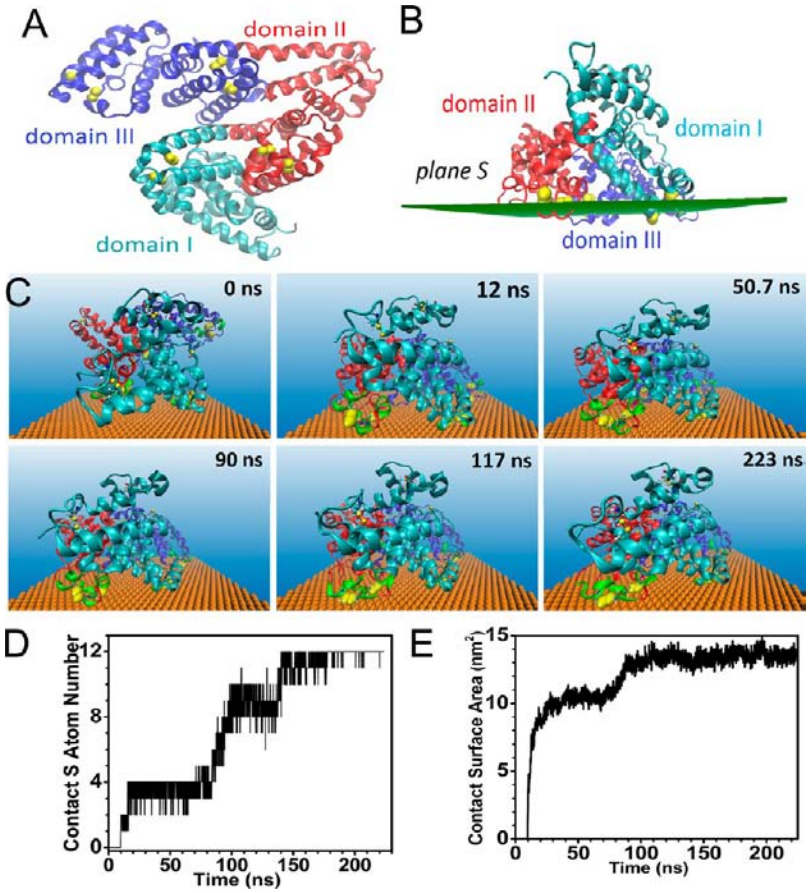

Figure 2. Interaction between AuNRs and BSA using MD simulation from 0 to 223 ns. (A) Crystal structures of BSA and the sulfur atoms around *plane S* (bottom view) and (B) those around *plane S* (depicted as green plane, side view). (C) Representative temporal snapshots of BSA binding to the gold surface. The unfolding secondary structures are highlighted in green. (D,E) Number of sulfur atoms in contact and contact surface area of an individual BSA on the gold surface accompanying with time. In (A–C), BSA is rendered as a cartoon representation and the three domains are colored cyan, red, and blue. The sulfur atoms are highlighted in a van der Waals representation and colored yellow.

surface and to form Au–thiol coordination bonds (Au–S). A stable serum protein corona on AuNRs (FBS/AuNRs) can effectively prevent direct contact of AuNRs with the cell membrane and reduce their cytotoxicity. These combined approaches offer an advantage to the study of the interfacial interactions of a protein corona with AuNRs, which helps us better understand the nature of the protective effects of the corona.

2. RESULTS AND DISCUSSION

Characterization of CTAB/AuNRs and BSA Corona-Coated AuNRs (BSA/AuNRs). CTAB/AuNRs were prepared according to previously published procedures.[17,51] Mean sizes were obtained by measuring 100 NRs using transmission electron microscopy (TEM). CTAB/AuNRs had an aspect ratio of 4.2, with a mean length of 55.6 ± 7.8 nm and width of 13.3 ± 1.8 nm (Supporting Information (SI), Figure S1). TEM images showed a thinner organic layer immediately surrounding the AuNRs and a thicker one after protein adsorption (Figure 1A,B). The thinner layer was a CTAB bilayer about 1.5 nm thick, and the thicker one was the BSA corona, about 5 nm thick.

In order to better understand the interaction of AuNRs with the protein corona, we lowered the surface coverage of the CTAB bilayer on the gold surface, thus leaving some bare gold surface for protein adsorption. When CTAB/AuNRs were centrifuged and rinsed twice, a part of the gold surface was directly exposed to the aqueous environment. Our previous results indicated that AuNRs with more complete CTAB coatings had higher surface charges (zeta potential about 35 mV), while those with lower CTAB coverage had lower surface charges to be 29.3 mV (Table S3).[19,26] CTAB/AuNRs were incubated with 0.5% BSA in PBS at 37 °C for 3 h and the resulting NP–protein complexes were separated from excess BSA by centrifugation twice at 12 000 rpm for 10 min and resuspended with deionized water to remove the unbound proteins. The zeta potential of CTAB/AuNRs was about +29.3 ± 0.7 mV, and that of BSA/AuNRs in water was about −18.6 ± 1.2 mV. The adsorbed protein coronas were then used to study their binding structure and stability on AuNRs and the cellular responses to them.

Interaction between a BSA Corona and AuNRs. We used the K-edge XANES of sulfur to study the possible adsorption mode of corona on AuNRs. Cysteine, methionine (Met), and cystine represent the three main forms of sulfur in BSA, with sulfur species consisting of R–S–H, R–S–R, and S–S, respectively. The first two species are similar to thiol, but the third one is distinct from the others.[35,38] Sulfur K-edge XANES information is sensitive to oxidation states, and the species of the element can be determined from the peak of the first derivative of XANES, the inflection point energy (IPE).[38] As indicated by the results of XANES and its first derivative,

dx.doi.org/10.1021/ja406924v | J. Am. Chem. Soc. 2013, 135, 17359–17368

there were three types of sulfur species in our system: thiol (R−S−H, R−S−R thiol), disulfide (S−S), and Au−thiol coordination (Au−S). The IPE values of cysteine, thiol, and methionine (Met) are 2473.1 eV, and those of disulfide (cystine) and Au-thiol are 2472.1 and 2472.6 eV, respectively (Figures S2A and 1C). Least-squares fitting of XANES indicated that when the AuNRs were incubated with cysteine or cystine, Au−S bonds were formed, while incubation with Met did not result in Au−S bonds, suggesting that the disulfides in BSA probably form Au−S coordination as cystines (Figures 1D and S4).

Disulfide bonds are the major form of sulfur in BSA. They are responsible for maintaining the protein's structure by stabilizing the α-helix bundles. BSA contains 17 disulfides (34 cysteine residues), one free thiol (a cysteine residue), and five Met (Figure S3A). When BSA was allowed to interact with AuNRs, the characteristics of its XANES spectra changed (Figure S2B). A least-squares linear combination fitting of XANES showed that adsorption of the BSA corona on AuNRs decreased the content of disulfides from 82% to 58% by inducing 26% of the sulfur atoms to transform into Au−S (Figure 1E), while the content of the R−S form, including Met or cysteine, decreased only slightly, from 18% to 16%.

The changes in BSA sulfur species from S−S to Au−S suggested that the interaction of BSA with AuNRs includes initial electrostatic adsorption followed by Au−S coordination (Figure 1F), which determines the transformation in secondary structures (see below). It has been reported that both thiol groups and organic disulfides are prone to forming Au−S coordination on the gold surface.[52,53] Although Au L_{III}-edge XANES did not show any changes in the chemical form of gold in AuNRs, this failure to observe changes is probably because the ratio of coordinated gold atoms to total atoms in the AuNRs would be quite low, less than 0.16%. This rate would be below the level of detection in XANES, so it is not practical to study the coordination structure of Au−S by extended XAFS or to distinguish changed gold species by XANES (Figure 1G, and discussion in SI). It is important to note that there are a variety of adsorption modes on AuNPs for different proteins. For example, a cysteine-free protein, ubiquitin, can be adsorbed on AuNP by short-range and non-electrostatic interactions as indicated by NMR and MD simulation.[31] Therefore, we also used CD to analyze the changes in secondary structures of a BSA corona. The secondary structures of BSA were determined in both an aqueous buffer solution and a corona on AuNRs (Figure 1H). For pristine BSA in a buffer solution, the measured contents of α-helix, β-sheet, β-turn, and random coil were 46%, 15%, 8.3%, and 30%, respectively. Upon incubation with CTAB/AuNRs, the corresponding structures of the adsorbed BSA corona changed to 36%, 37.6%, 0, and 26.4% at 0.5 h; 38%, 35.9%, 0, and 26.1% at 1 h; and 32.9%, 41.9%, 1.1%, and 24.2% at 2 h, respectively. These rapid changes in the secondary structures of the BSA corona arose from the transformation of disulfide bonds to Au−S coordination.

MD Simulation for the Interaction of BSA and AuNRs. To better understand the interaction process in detail, we performed an MD simulation to study the possible interaction modes of BSA with the AuNR surface, together with the changes in the BSA protein conformation. The crystal structure of BSA reveals a heart-shaped protein (Figures 2A and S3A). It is composed of 585 residues with three structurally similar domains (I, II, and III), each of which can be further divided into two subdomains, A and B. BSA contains a high content of α-helical structure: For each domain there are 10 α-helices: α-helices 1−6 (h1−h6) belonging to subdomain A and helices 7−10 (h7−10) to subdomain B (Figure S3B). In both domains II and III, there are 6 disulfide bonds connecting the helices, organized into three pairs: disulfide bonds connecting h1-h3 and h3-h4, h4-h5 and h5-h6, and h7-h9 and h9-h10 separately. For each pair, the separation of disulfide bonds is less than 7.5 Å. In domain I, the disulfide bond connecting h1 and h3 is missing, and there is a free cysteine 34 instead. Altogether, there are 35 cysteine residues in BSA. We noted that the disulfide bond pairs of h7-h9 and h9-h10 in domain I, h4-h5 and h5-h6 in domain II, and h1-h3 and h3-h4 in domain III are distributed in the same plane (denoted *plane S*), arising from the three-fold symmetry of BSA. Moreover, the disulfide bond pairs h7-h9 and h9-h10 in domain III are also located in this plane. In this way, we have successfully identified *plane S*, consisting of eight disulfide bonds, which can serve as the candidate binding surface with AuNRs (Figures 2B and S3B).

In addition, we performed an MD simulation for 223 ns to probe the adsorption of BSA to the Au (111) plane and the concomitant conformational change. In the simulation, the BSA was initially placed with *plane S* parallel to the gold surface continually. A driving force of 100 pN was applied to the sulfur atoms in *plane S* to accelerate the adsorption process. Once the sulfur atoms were in direct contact with the gold surface, they were restrained in their positions by a harmonic potential to mimic chemical adsorption. The adsorption process and final configurations of BSA adsorbed on the Au (111) plane are shown in Figures 2C and S5, and Movies 1 and 2 (.mpg) in the SI. In BSA, the disulfide bonds were mainly located at the ends of the two α-helices and were relatively exposed to the solvent. For each disulfide bond pair on *plane S*, there was at least one cysteine residue whose solvent-accessible surface area was larger than 18 $Å^2$. The solvent accessibility of the disulfide bonds facilitated their adsorption onto the gold surface; the number of sulfur atoms in direct contact with the gold surface continuously increased to 12 at t = 140 ns (Figure 2D and Table S1). Such an adsorption mode may result in the reduction of as many as six disulfide bonds, accounting for 35% of the disulfide bonds in BSA. The sulfur XANES results for the BSA on AuNRs indicated that about 24% of the disulfide bonds were reduced after adsorption. It should be noted that not all the BSA in solution can be adsorbed onto AuNRs and make sufficient contact with the gold surface. In this way, the ratio of reduced sulfur atoms in the experiment should be lower than the ideal situation. On the other hand, the disulfide bonds C123−C168 and C433−C444, which connect h7-h9 in domain I and h3-h4 in domain III, also located in *plane S*, were not observed to contact the gold surface during the whole 223 ns simulation. It is important to note that the time scale of the MD simulation is still too short due to limitations of computational power. We cannot entirely exclude the possible adsorption of disulfide bonds C123−C168 and C433−C444 at longer times.

The conformational change of BSA occurs during the process of adsorption of disulfide bonds. Even though the sulfur atoms in *plane S* were relatively exposed, a change in local structure was still required to achieve further exposure and subsequent binding of the sulfur atoms. Moreover, the conformation of BSA continuously changed even after all six of the disulfide bonds were bound to the gold surface at t = 140 ns. The adsorption of BSA onto the gold surface induced additional conformational changes to form an extended contact surface area (Figure 2E). The change in secondary structure mainly reflects the unfolding of α-helices, especially in the region

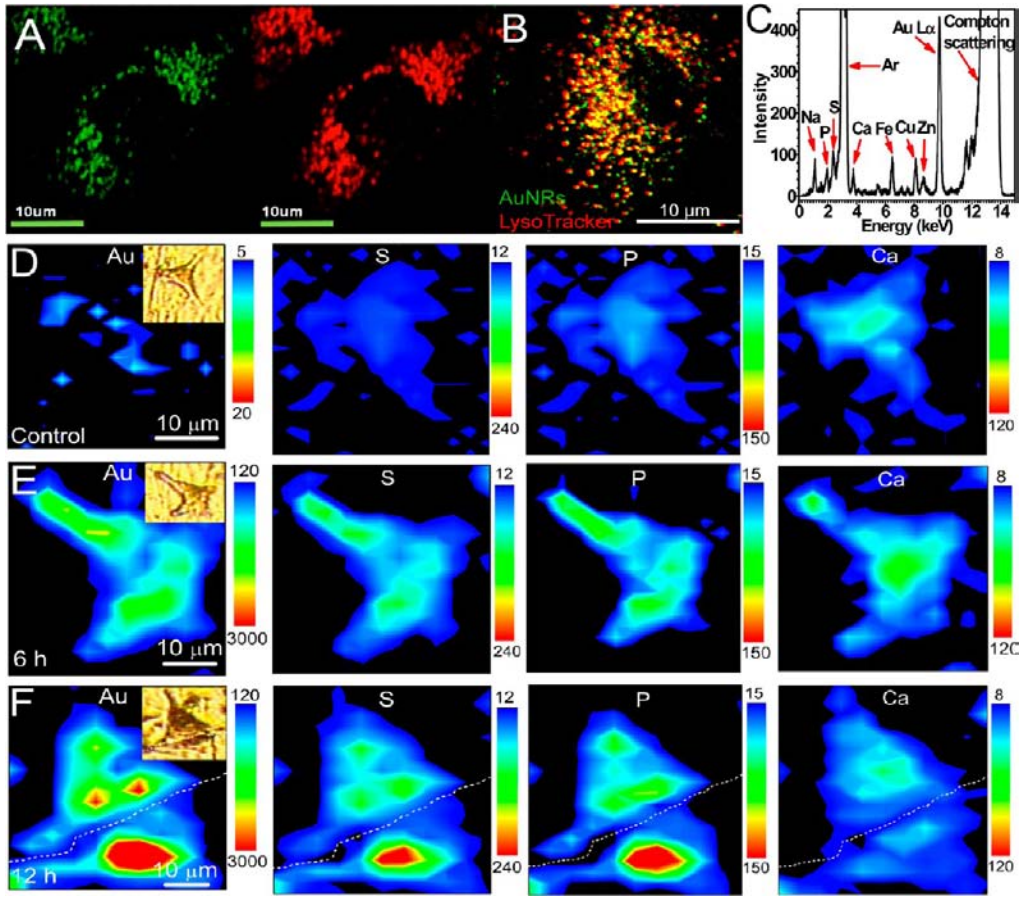

Figure 3. Elemental mapping and microscopic images for AuNRs in a single cell. (A) Two-photon fluorescence images of AuNRs in a live A549 cell, excited at 780 nm and detected at 520 nm (green) and 560 nm (red). (B) Colocalization of AuNRs (green) and lysosomes (red) stained by LysoTracker Red. (C) Main element analysis of a random spot in A549 cells exposed to 50 μM FBS/AuNRs for 6 h, using XRF spectroscopy. Fluorescence intensities of the elements Na, S, P, Ca, Fe, Cu, and Zn are shown as Kα lines, while Au is shown as an Lα line. (D–F) Elemental mapping of Au, S, P, and Ca using μ-XRF to analyze internalized FBS/AuNRs in cells at different time intervals. The insets are cell images under a bright field.

around the bound disulfide bond pairs: The N-terminus of helix 10 in all three domains and helices 5 and 6 in domain II were largely unfolded. In general, the α-helical content of BSA decreased in the final configuration, which is consistent with the experimental observations from the CD spectrum. It is worth noting that the structure of BSA is relatively flexible because of the large α-helix content, and that flexibility essentially facilitates sufficient adsorption of BSA on the gold surface.

The SR technique in combination with MD simulation offers a remarkable advantage in characterizing binding stability and the corresponding structure of protein coronas. Stable adsorption of the BSA corona arising from chemical adsorption on AuNRs is attributed to the Au–S bonds, which can be captured by XANES. Moreover, MD simulation successfully identifies the binding interface of BSA and the process of adsorption and concomitant conformational change. The simulation results about the adsorbed sulfur atoms are consistent with the experimental observations. This integrated methodology for revealing binding structures of BSA may be helpful for future studies about the protein corona. It has been widely accepted that the differences in the properties of proteins, such as the rigidity, shape, and the functional group distribution in the interior or on the surface of NPs, can influence the binding structures of proteins. The effects of such differences should be taken into account in the further research about the other proteins in the corona.

Adsorption of serum protein onto AuNRs may interrupt the direct interaction of AuNRs with membrane proteins. There are at least 12 Au–thiol bonds that contribute to the binding of BSA on AuNRs. This large number of bonds should result in a remarkably stable adsorption of BSA, leading to highly reduced cytotoxicity before AuNRs enter the cell. The binding structures may account for some biological impacts of these FBS-coated AuNPs, e.g., endocytosis and cytotoxicity.[11,24,27,28,50] In our system, BSA is adsorbed on AuNRs in a "side-on" orientation, and the binding interface around *plane S* should be different from the adsorption of BSA as driven by electrostatic attraction and other forces.

Interaction of the Serum Protein Corona-Coated AuNR (Denoted FBS/AuNR) Complex with Cells. Once the serum protein corona forms on AuNRs, the complex can be recognized by A549 cell, a human lung adenocarcinoma epithelial cell line and triggers a series of responses, i.e., uptake, translocation, accumulation or exclusion, changes in cellular metabolism levels, and cell death.[19,55] Here, we used *z*-axis scanning imaging by two-photon confocal microscope to observe that a large number of AuNRs were internalized within cells (Figure 3A and Movie 3 (.avi) in SI). According to the co-localization results, most of the AuNRs were localized in the

dx.doi.org/10.1021/ja406924v | J. Am. Chem. Soc. 2013, 135, 17359–17368

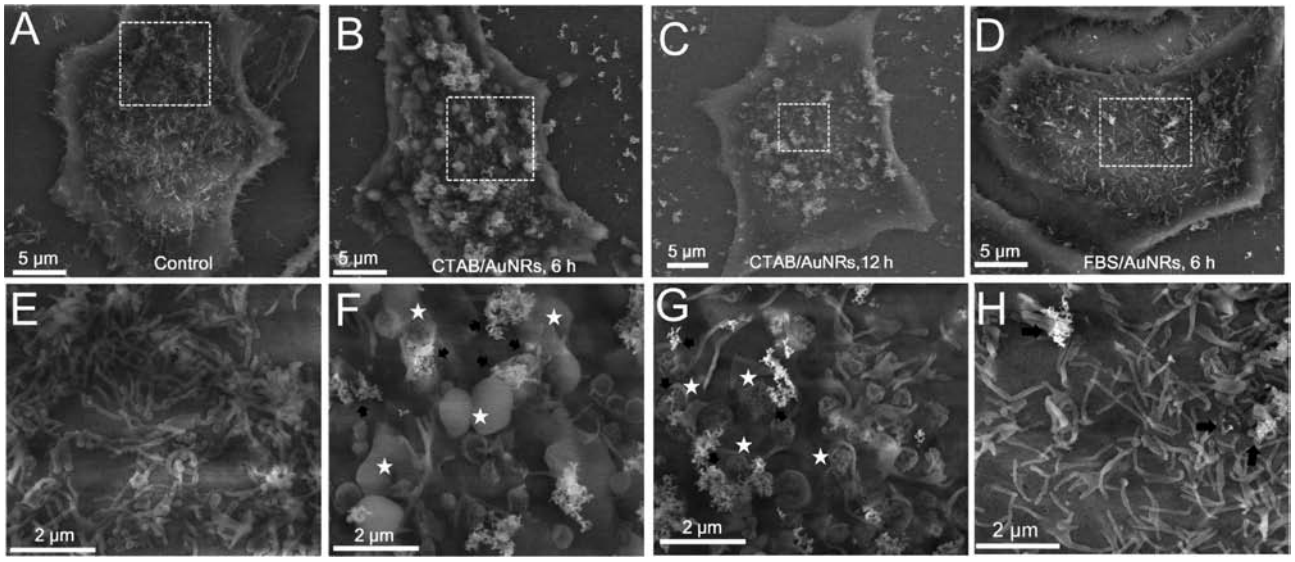

Figure 4. ESEM images for cytoplasmic membrane structures in serum-free medium: (A,E) untreated A549 cells; (B,F; C,G) cells exposed to 50 μM AuNRs for 6 and 12 h, respectively; and (D,H) cells exposed to 50 μM FBS corona-coated AuNRs for 6 h. The upper figures (A−D) represent a whole cell image, and zoom-ins of the areas in white dashed-line boxes are shown below (E−H). In (E−H), the black arrows and the white stars mark AuNRs and blebs on membranes, respectively.

lysosomes (Figure 3B). During cellular uptake, FBS/AuNRs may carry a variety of extracellular proteins into cells. Hence, it is still a challenge to thoroughly characterize the FBS corona on AuNRs within cells. As will be discussed below, the μ-XRF technique is a powerful technique for studying the adsorption mode. The spectrum can be used as an elemental fingerprint based on the characteristic X-ray absorption energies (Figure 3C). It can also collect the intensities of fluorescence signals, which are proportional to the concentrations of elements within the sample. Therefore, μ-XRF can be used to identify elements and to semiquantify the content of multiple elements simultaneously.

In this work, the intracellular distribution of FBS/AuNRs was studied by elemental mapping and semiquantitative analysis of Au, S, and P. Internalized amounts of FBS/AuNRs were roughly estimated by comparing the fluorescence intensities of Au, S, and P to those in untreated cells. The fluorescence intensities of Au, S, and P in a single cell increased with time after exposure to FBS/AuNRs for 12 h as shown in Figure 3D−F. The values of the Au, S, and P content at 12 h increased by 1.4-, 1.4-, and 1.3-fold, respectively, compared to those at 6 h (Table S2). The increased amounts of intracellular S and P were mainly accounted for by proteins or peptides containing sulfur and membrane or vesicles containing phospholipids, respectively. This result indicates the internalization of AuNRs accompanying FBS proteins and the formation of vesicles around FBS/AuNRs during endocytosis. These observations about the internalization of AuNRs were also supported by previous results from inductively coupled plasma mass spectrometry (ICP-MS).[19] Moreover, the elemental mappings confirmed that the distributions of Au, S, and P were roughly identical, which further supports the observation that the internalization of the FBS/AuNR complex is correlated with vesicle formation. Interestingly, the main distribution of Au, S, and P is different from that of Ca, which is mainly distributed in the nucleus suggesting that intracellular AuNRs are mainly distributed in lysosomes around the nucleus (Figure 3B,D−F). Thus, μ-XRF mapping combined with confocal microscope imaging with high spatial resolution provides a novel, convenient and sensitive approach to studying the distribution of FBS/AuNRs in cells.

The above results suggest a possible process for the adsorption of the serum protein corona onto AuNRs. Initially, electrostatic forces drive proteins to approach the gold surface due to the opposite surface charges of the protein and AuNRs (Table S3). The direct adsorption is then mainly driven by chemisorptive forces: binding of sulfur atoms in cystine or disulfide bonds to the gold surface via Au−S bonds. As revealed by μ-XRF, FBS/AuNRs were then internalized by cells as a whole, with the corona intact, as indicated by a good co-localization for gold (AuNRs) and sulfur elements (proteins) (Figure 3D−F). Thus SR-based analysis techniques offer a powerful approach to exploring the interaction between NPs and biological interfaces.

Protective Effects of the Serum Protein Corona against Direct Damage to Cell Membranes. We previously reported that CTAB/AuNRs can decrease the integrity of the lysosomal membrane of A549 cells and cause a leaky membrane structure once the adsorbed serum protein corona detaches from the AuNRs and the CTAB bilayer is exposed.[19] To confirm that the serum corona plays a protective role when AuNRs contact the membrane, we examined the impact of FBS/AuNRs and CTAB/AuNRs on the cytoplasmic membrane structure. By incubating cells with the two types of AuNRs in a serum-free culture medium, we obtained microscopic images that provided evidence for the protective effects of the serum protein corona (Figure 4). Untreated cells had intact membrane surfaces covered with numerous long microvilli as shown by an environmental scanning electronic microscope (ESEM) (Figure 4A,E). After exposure to 50 μM CTAB/AuNRs in serum-free medium for 6 h, the microvilli decreased substantially in number and even disappeared. Meanwhile, CTAB/AuNRs aggregated on the membrane, and large blebs appeared around them (Figure 4B,F). At 12 h, many blebs were still visible on the membrane but some obvious defects appeared in the blebs (Figure 4C,G). The appearance of blebs

dx.doi.org/10.1021/ja406924v | J. Am. Chem. Soc. 2013, 135, 17359−17368

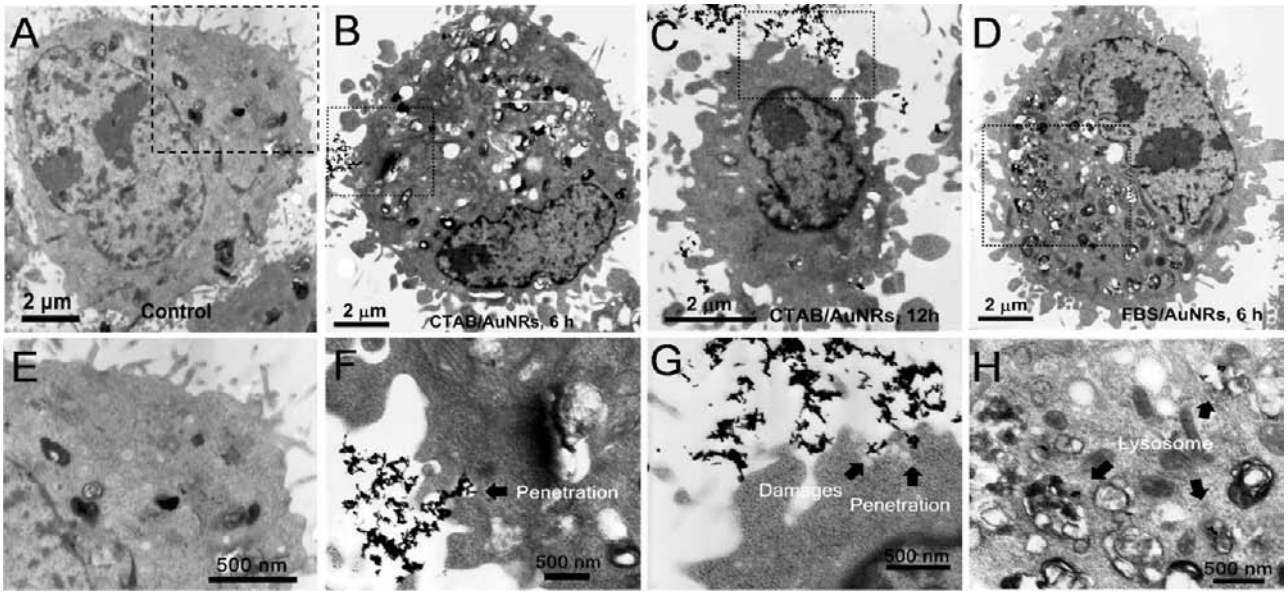

Figure 5. TEM images for cytoplasmic membrane and intracellular ultrastructures in serum-free medium: (A,E) untreated A549 cells; (B,F; C,G) cells exposed to 50 μM AuNRs for 6 and 12 h, respectively; and (D,H) cells exposed to 50 μM FBS corona-coated AuNRs for 6 h. The upper figures (A–D) represent a whole cell image, and zoom-ins of the areas in black dashed-line boxes are shown below (E–H). In (F–H), the black arrows indicate AuNRs near or inside membrane structures.

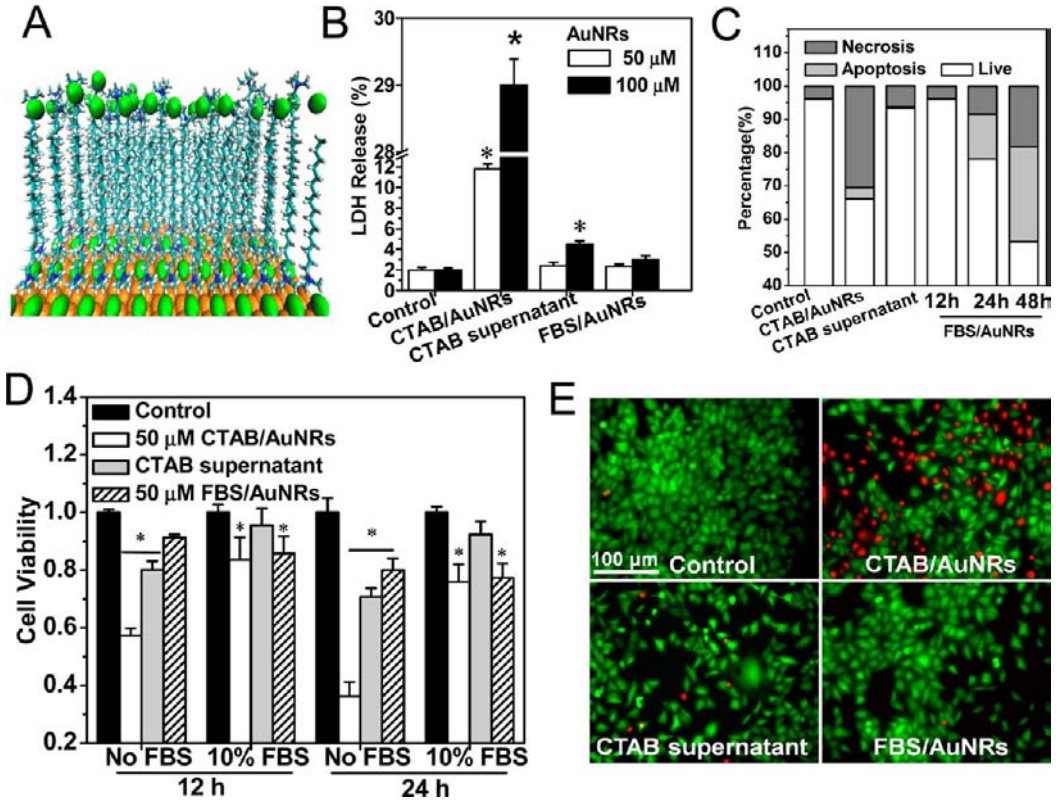

Figure 6. Protective effects of protein corona on the membrane integrity and cell viability. (A) Representative snapshots of a CTAB bilayer assembled on the Au (111) surface based on MD simulation. The gold, blue, and green colors indicate Au, N, and Br atoms, respectively. (B) LDH release from cells exposed to CTAB/AuNRs, CTAB supernatant solution, and FBS-coated AuNRs for 24 h. Cytotoxicity was evaluated by an apoptosis and necrosis ratio analysis using flow cytometry (C), by a mitochondrial dehydrogenase activity assay using a CCK-8 assay (D), and by a live–dead assay (E) for cells exposed to CTAB/AuNRs, CTAB supernatant, and FBS/AuNRs at 12 and 24 h. * indicates significant effects of AuNRs on cells ($p < 0.05$). Results are described as mean values and standard deviations, $N = 3$.

on the membrane of the epithelial cells indicated an immediate response to the toxic stimulus.[56,57] We observed that the sizes of the blebs decreased and the shape changed from swollen to atrophic with time (Figure 4B,C). Thus early exposure to CTAB/AuNRs induces the formation of swollen blebs on the membrane, while the subsequent interaction of CTAB/AuNRs

dx.doi.org/10.1021/ja406924v | J. Am. Chem. Soc. 2013, 135, 17359–17368

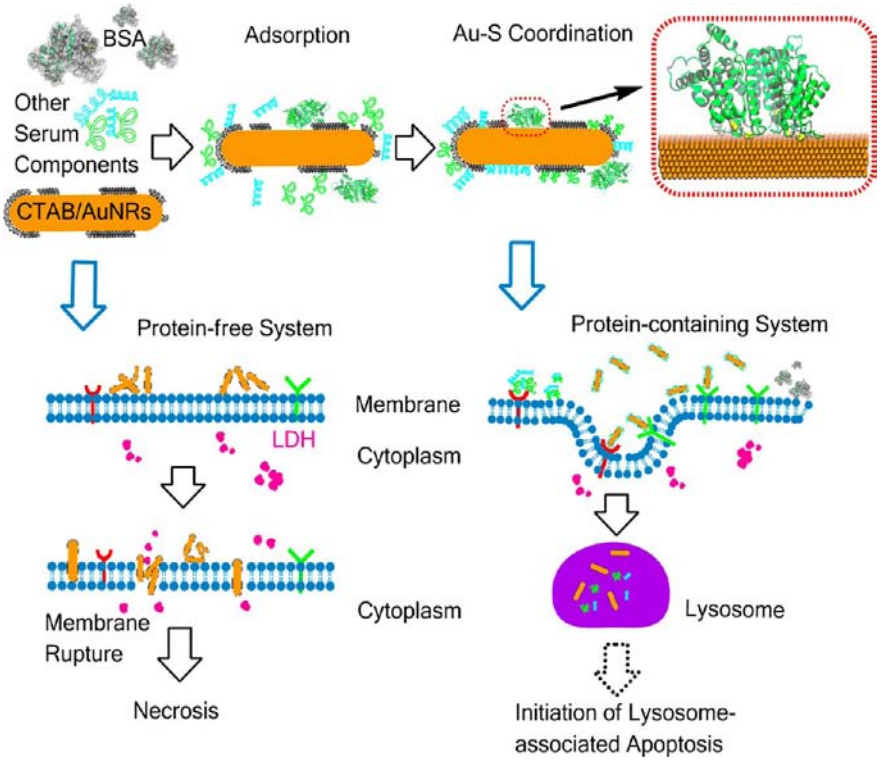

Figure 7. Role of serum proteins in the interaction of AuNRs with membranes. Partially exposed CTAB/AuNRs are incubated with BSA to form a hard BSA corona via Au−S coordination. The existence of the protein corona facilitates the protein receptor-mediated internalization and translocation of AuNRs to endo-/lysosomes, where the CTAB bilayer on AuNRs can probably induce lysosome-associated apoptosis. Without a protein coating, CTAB/AuNRs can directly destroy the cytoplasmic membrane, form defects, and cause the release of LDH, which eventually induces necrosis.

with the membrane has destructive effects on the blebs. In contrast, FBS/AuNRs did not cause dramatic effects on membrane structures (Figure 4D,H). Moreover, the serum protein corona improved the stability of AuNRs in serum-free medium from the decreased number of AuNR aggregates on the cell surface (Figure 4B,C vs D, and F,G vs H).

TEM imaging also clearly indicates time-dependent changes in membrane structures after treatment with CTAB/AuNRs (Figure 5). The cytoplasmic membrane became thinner, CTAB/AuNRs penetrated into the membrane, and membrane structures became damaged, along with an increase in the number of blebs and a loss of microvilli (Figure 5A−C and E−G). For FBS/AuNRs, membrane structures remained intact, and a few AuNRs could be found around the plasma membrane, mainly localized within vesicles like endo-/lysosomes (Figure 5D,H). Taken together, the TEM and ESEM results support the conclusion that the serum protein corona not only increases the stability of AuNRs, but also prevents their directly destructive effects on membrane structures.

As surfactants, CTAB molecules assemble on AuNRs during the synthesis and form a bilayer structure,[58] in the upper layer the hydrophilic head groups point toward the aqueous medium and the hydrophobic chains point toward the NR core (Figure 6A). The CTAB molecules share an amphipathic nature with lipid molecules, which could be the reason why CTAB/AuNRs seriously disturb the cytoplasmic or lysosomal membranes. As a result, CTAB/AuNRs induce the release of lactic acid dehydrogenase (LDH) from the cytoplasm due to reduced membrane integrity in a dose-dependent manner similarly as reported previously.[50] In contrast, FBS/AuNRs do not cause membrane impairment within a 24 h time frame (Figure 6B).

We also examined subsequent cell responses to AuNRs such as apoptosis or necrosis, metabolism, and cell survival due to decreased integrity of the cell membranes. The plasma membrane acts as a barrier that prevents a direct disturbance from extracellular stimulation and maintains homeostatic conditions within the cell. Disturbance in the cell membranes by CTAB/AuNRs results in a high percentage of necrosis and some apoptosis, as shown by the Annexin V-PI assay (Figure 6C). CTAB/AuNRs also decrease mitochondrial metabolism activity or cell viability based on the CCK-8 assay similarly as reported.[19,50] Here, a central role is played by the CTAB/AuNRs rather than the CTAB released from CTAB/AuNRs. Interestingly, such negative effects on the membrane decrease after a hard FBS corona is formed (Figure 6D). We found that the stability of FBS corona on the surface of AuNRs is inversely correlated with the cytotoxicity of CTAB/AuNRs determined by LDH assay (Figure S6). Meanwhile, in a 10% FBS medium, the toxicity of CTAB/AuNRs is the same as FBS/AuNRs. As indicated above, the designed BSA corona and the naturally occurring FBS/AuNRs reduce cellular toxicity of CTAB/AuNRs similarly. However, both FBS/AuNRs and CTAB/AuNRs cause slightly time-dependent toxicity rather than immediate toxicity (Figure 6C,D), possibly due to later exposure of CTAB.[19] As a result, CTAB/AuNRs cause acute toxicity and induce cell death, as shown by the live−dead assay results (Figure 6E).

To decrease interaction of the CTAB bilayer with cell membranes, the BSA corona was formed after centrifuging CTAB/AuNRs twice to expose some bare Au surface for BSA

dx.doi.org/10.1021/ja406924v | J. Am. Chem. Soc. 2013, 135, 17359−17368

adsorption. BSA forms a hard corona on the gold surface via Au−S coordination that increases the colloidal stability of the corona−NPs in the physiological fluids.[59] Serum protein coronas prevent a direct interaction between the cell membrane and the CTAB bilayer on the surface of the AuNRs, thus averting damage to the cell membrane (Figure 7). However, most of serum protein coronas can dissociate from the surface and undergo enzymatic degradation when the corona−NPs move into digestive organelles such as lysosomes,[59,60] and the re-exposed toxic surface may then decrease the lysosomal membrane integrity[18,19] and cause lysosome-mediated apoptosis.[18,59] In contrast, when the corona is not present, the exposure of the cell membrane to CTAB/AuNRs the causes the release of LDH and eventually induces necrosis. Thus the protein corona regulates the biological effects of CTAB/AuNRs, which are closely related to the stability of adsorption.

3. CONCLUSIONS

To summarize, we designed a hard BSA corona on the surface of AuNRs and successfully identified the binding structure of the BSA corona. The adsorption of BSA formed a stable corona on the AuNRs that was attributed to at least 12 Au−S bonds with side-on binding modes. The stable BSA corona should contribute to the stability of an FBS corona and reduce the acute toxicity of NPs by suppressing potentially destructive effects on the cell membrane. It is worth emphasizing that a methodology combining SR techniques with computational simulation can realize detailed characterization of the binding structure of the protein corona on NPs. The strategy will definitely help us understand interfacial interactions among proteins, NPs, and cell membranes, and their potential impact on cell responses. These findings and the integrated strategy will provide guidance not only for the study of the interaction between NPs and biological interfaces, but also for the rational design of nanomaterials for safe and effective applications in biomedicine.

■ ASSOCIATED CONTENT

Supporting Information

Crystal structures of BSA; process of cysteine residues attaining in direct contact with the gold surface; changes in related contents of intracellular Au, S, and P based on XRF; characterization of AuNRs using TEM; structural fingerprints as inflection point energy of S K-edge XANES; binding of cysteine and BSA to the gold surface using MD simulation; movies showing the interaction of AuNRs and BSA; discussion of the results of gold L_{III} edge XANES; experimental details, including the preparation of AuNRs, BSA/AuNRs, and FBS/AuNRs, characterization of AuNRs, procedures for XANES and micro-XRF analysis, MD simulation, microscopic imaging of cells, analysis of cell membrane integrity, cell viability, and apoptosis/necrosis, and the live−dead assay. This material is available free of charge via the Internet at http://pubs.acs.org.

■ AUTHOR INFORMATION

Corresponding Authors

wuxc@nanoctr.cn
chenchy@nanoctr.cn

Author Contributions

‡L.W. and J.L. contributed equally.

Notes

The authors declare no competing financial interest.

■ ACKNOWLEDGMENTS

This work was financially supported by the National Basic Research Program of China (2011CB933401, 2010CB934004, 2013CB933704, and 2012CB934000), the National Natural Science Foundation of China (21320102003, 11205166 and 31070854), and the Major Equipment Program (2011YQ030134). The work was performed under the Photon Factory in KEK, Japan, the BSRF in Beijing, and the SSRF in Shanghai. We thank Prof. Masaharu Nomura and Dr. Yoshinori Kitajima at KEK, Prof. Yidong Zhao at BSRF, and Prof. Yuying Huang at SSRF for the XANES experiments, Dr. Wei Xu and Dr. Jiating Zhao at BSRF for fruitful discussions and data analysis of the XANES spectra, and Prof. Atsuo Iida at KEK and Prof. Aiguo Li for the μ-XRF experiment. We are grateful to Prof. Dong Han and Mrs. Jiayi Xie at NCNST for the ESEM experiments. We also thank Dr. Xiaofeng Wang at IHEP for manuscript preparation.

■ REFERENCES

(1) Nel, A. E.; Madler, L.; Velegol, D.; Xia, T.; Hoek, E. M. V.; Somasundaran, P.; Klaessig, F.; Castranova, V.; Thompson, M. *Nat. Mater.* **2009**, *8*, 543−557.

(2) Monopoli, M. P.; Aberg, C.; Salvati, A.; Dawson, K. A. *Nat. Nanotechnol.* **2012**, *7*, 779−786.

(3) Walkey, C. D.; Olsen, J. B.; Guo, H.; Emili, A.; Chan, W. C. W. *J. Am. Chem. Soc.* **2011**, *134*, 2139−2147.

(4) Laera, S.; Ceccone, G.; Rossi, F.; Gilliland, D.; Hussain, R.; Siligardi, G.; Calzolai, L. *Nano Lett.* **2011**, *11*, 4480−4484.

(5) Ge, C. C.; Du, J. F.; Zhao, L.; Wang, L. M.; Liu, Y.; Li, D. H.; Yang, Y. L.; Zhou, R. H.; Zhao, Y. L.; Chai, Z. F.; Chen, C. Y. *Proc. Natl. Acad. Sci. U.S.A.* **2011**, *108*, 16968−16973.

(6) Hu, W. B.; Peng, C.; Lv, M.; Li, X. M.; Zhang, Y. J.; Chen, N.; Fan, C. H.; Huang, Q. *ACS Nano* **2011**, *5*, 3693−3700.

(7) Lundqvist, M.; Stigler, J.; Elia, G.; Lynch, I.; Cedervall, T.; Dawson, K. A. *Proc. Natl. Acad. Sci. U.S.A.* **2008**, *105*, 14265−14270.

(8) Milani, S.; Baldelli Bombelli, F.; Pitek, A. S.; Dawson, K. A.; Rädler, J. *ACS Nano* **2012**, *6*, 2532−2541.

(9) Monopoli, M. P.; Walczyk, D.; Campbell, A.; Elia, G.; Lynch, I.; Baldelli Bombelli, F.; Dawson, K. A. *J. Am. Chem. Soc.* **2011**, *133*, 2525−2534.

(10) Tedja, R.; Lim, M.; Amal, R.; Marquis, C. *ACS Nano* **2012**, *6*, 4083−4093.

(11) Zhu, Z. J.; Posati, T.; Moyano, D. F.; Tang, R.; Yan, B.; Vachet, R. W.; Rotello, V. M. *Small* **2012**, *8*, 2659−2663.

(12) Lesniak, A.; Fenaroli, F.; Monopoli, M. P.; Åberg, C.; Dawson, K. A.; Salvati, A. *ACS Nano* **2012**, *6*, 5845−5857.

(13) Lesniak, A.; Salvati, A.; Santos-Martinez, M. J.; Radomski, M. W.; Dawson, K. A.; Åberg, C. *J. Am. Chem. Soc.* **2013**, *135*, 1438−1444.

(14) Li, Y. F.; Chen, C. Y. *Small* **2011**, *7*, 2965−2980.

(15) Maiorano, G.; Sabella, S.; Sorce, B.; Brunetti, V.; Malvindi, M. A.; Cingolani, R.; Pompa, P. P. *ACS Nano* **2010**, *4*, 7481−7491.

(16) Larson, T. A.; Joshi, P. P.; Sokolov, K. *ACS Nano* **2012**, *6*, 9182−9190.

(17) Wang, L. M.; Li, Y. F.; Zhou, L. J.; Liu, Y.; Meng, L.; Zhang, K.; Wu, X. C.; Zhang, L. L.; Li, B.; Chen, C. Y. *Anal. Bioanal. Chem.* **2010**, *396*, 1105−1114.

(18) Wang, F.; Yu, L.; Monopoli, M. P.; Sandin, P.; Mahon, E.; Salvati, A.; Dawson, K. A. *Nanomedicine* **2013**, *9*, 1159−1168.

(19) Wang, L. M.; Liu, Y.; Li, W.; Jiang, X. M.; Ji, Y. L.; Wu, X. C.; Xu, L. G.; Qiu, Y.; Zhao, K.; Wei, T. T.; Li, Y. F.; Zhao, Y. L.; Chen, C. Y. *Nano Lett.* **2011**, *11*, 772−780.

(20) Deng, Z. J.; Liang, M.; Monteiro, M.; Toth, I.; Minchin, R. F. *Nat. Nanotechnol.* **2011**, *6*, 39−44.

(21) Sun, C. J.; Yang, H.; Yuan, Y.; Tian, X.; Wang, L. M.; Guo, Y.; Xu, L.; Lei, J. L.; Gao, N.; Anderson, G. J.; Liang, X. J.; Chen, C. Y.; Zhao, Y. L.; Nie, G. J. *J. Am. Chem. Soc.* **2011**, *133*, 8617−8624.

(22) Kah, J. C. Y.; Chen, J.; Zubieta, A.; Hamad-Schifferli, K. *ACS Nano* **2012**, *6*, 6730−6740.
(23) Gradishar, W. J.; Tjulandin, S.; Davidson, N.; Shaw, H.; Desai, N.; Bhar, P.; Hawkins, M.; O'Shaughnessy, J. *J. Clin. Oncol.* **2005**, *23*, 7794−7803.
(24) Hühn, D.; Kantner, K.; Geidel, C.; Brandholt, S.; Cock, I. D.; Soenen, S. J. H.; Rivera Gil, P.; Montenegro, J. M.; Braeckmans, K.; Müllen, K.; Nienhaus, G. U.; Klapper, M.; Parak, W. J. *ACS Nano* **2013**, *7*, 3253−3263.
(25) Hauck, T. S.; Ghazani, A. A.; Chan, W. C. *Small* **2008**, *4*, 153−159.
(26) Qiu, Y.; Liu, Y.; Wang, L. M.; Bai, R.; Ji, Y. L.; Wu, X. C.; Zhao, Y. L.; Li, Y. F.; Chen, C. Y. *Biomaterials* **2010**, *31*, 1139−1147.
(27) Salvati, A.; Pitek, A. S.; Monopoli, M. P.; Prapainop, K.; Bombelli, F. B.; Hristov, D. R.; Kelly, P. M.; Aberg, C.; Mahon, E.; Dawson, K. A. *Nat. Nanotechnol.* **2013**, *8*, 137−143.
(28) Lai, Z. W.; Yan, Y.; Caruso, F.; Nice, E. C. *ACS Nano* **2012**, *6*, 10438−10448.
(29) Cedervall, T.; Lynch, I.; Lindman, S.; Berggård, T.; Thulin, E.; Nilsson, H.; Dawson, K. A.; Linse, S. *Proc. Natl. Acad. Sci. U.S.A.* **2007**, *104*, 2050−2055.
(30) Lacerda, S. H. D. P.; Park, J. J.; Meuse, C.; Pristinski, D.; Becker, M. L.; Karim, A.; Douglas, J. F. *ACS Nano* **2009**, *4*, 365−379.
(31) Brancolini, G.; Kokh, D. B.; Calzolai, L.; Wade, R. C.; Corni, S. *ACS Nano* **2012**, *6*, 9863−9878.
(32) Zhang, D.; Neumann, O.; Wang, H.; Yuwono, V. M.; Barhoumi, A.; Perham, M.; Hartgerink, J. D.; Wittung-Stafshede, P.; Halas, N. J. *Nano Lett.* **2009**, *9*, 666−671.
(33) Shang, L.; Wang, Y. Z.; Jiang, J. G.; Dong, S. J. *Langmuir* **2007**, *23*, 2714−2721.
(34) Mahmoudi, M.; Lynch, I.; Ejtehadi, M. R.; Monopoli, M. P.; Bombelli, F. B.; Laurent, S. *Chem. Rev.* **2011**, *111*, 5610−5637.
(35) Jalilehvand, F. *Chem. Soc. Rev.* **2006**, *35*, 1256−1268.
(36) Zhang, P.; Sham, T. K. *Phys. Rev. Lett.* **2003**, *90*, 245502−1−4.
(37) Qu, Y.; Li, W.; Zhou, Y. L.; Liu, X. F.; Zhang, L. L.; Wang, L. M.; Li, Y. F.; Iida, A.; Tang, Z. Y.; Zhao, Y. L.; Chai, Z. F.; Chen, C. Y. *Nano Lett.* **2011**, *11*, 3174−3183.
(38) Rompel, A.; Cinco, R. M.; Latimer, M. J.; McDermott, A. E.; Guiles, R. D.; Quintanilha, A.; Krauss, R. M.; Sauer, K.; Yachandra, V. K.; Klein, M. P. *Proc. Natl. Acad. Sci. U.S.A.* **1998**, *95*, 6122−6127.
(39) Chai, Z. F.; Zhang, Z. Y.; Feng, W. Y.; Chen, C. Y.; Xu, D. D.; Hou, X. L. *J. Anal. At. Spectrom.* **2004**, *19*, 26−33.
(40) Chen, C. Y.; Li, Y. F.; Qu, Y.; Chai, Z. F.; Zhao, Y. L. *Chem. Soc. Rev.* **2013**, *42*, 8266−8303.
(41) Vairavamurthy, A. *Spectrochim. Acta A: Mol. Biomol. Spectrosc.* **1998**, *54*, 2009−2017.
(42) Bohic, S.; Murphy, K.; Paulus, W.; Cloetens, P.; Salome, M.; Susini, J.; Double, K. *Anal. Chem.* **2008**, *80*, 9557−9566.
(43) Corezzi, S.; Urbanelli, L.; Cloetens, P.; Emiliani, C.; Helfen, L.; Bohic, S.; Elisei, F.; Fioretto, D. *Anal. Biochem.* **2009**, *388*, 33−39.
(44) McRae, R.; Lai, B.; Vogt, S.; Fahrni, C. J. *J. Struct. Biol.* **2006**, *155*, 22−29.
(45) Wang, H. F.; Huff, T. B.; Zweifel, D. A.; He, W.; Low, P. S.; Wei, A.; Cheng, J. X. *Proc. Natl. Acad. Sci. U.S.A.* **2005**, *102*, 15752−15756.
(46) Huang, X. H.; El-Sayed, I. H.; Qian, W.; El-Sayed, M. A. *J. Am. Chem. Soc.* **2006**, *128*, 2115−2120.
(47) Zhang, Z. J.; Wang, L. M.; Wang, J.; Jiang, X. M.; Li, X. H.; Hu, Z. J.; Ji, Y. L.; Wu, X. C.; Chen, C. Y. *Adv. Mater.* **2012**, *24*, 1418−1423.
(48) Xu, L. G.; Liu, Y.; Chen, Z. Y.; Li, W.; Liu, Y.; Wang, L. M.; Liu, Y.; Wu, X. C.; Ji, Y. L.; Zhao, Y. L.; Ma, L. Y.; Shao, Y. M.; Chen, C. Y. *Nano Lett.* **2012**, *12*, 2003−2012.
(49) Alvarez-Puebla, R. A.; Agarwal, A.; Manna, P.; Khanal, B. P.; Aldeanueva-Potel, P.; Carbó-Argibay, E.; Pazos-Pérez, N.; Vigderman, L.; Zubarev, E. R.; Kotov, N. A.; Liz-Marzán, L. M. *Proc. Natl. Acad. Sci. U.S.A.* **2011**, *108*, 8157−8161.
(50) Wang, L. M.; Jiang, X. M.; Ji, Y. L.; Bai, R.; Zhao, Y. L.; Wu, X. C.; Chen, C. Y. *Nanoscale* **2013**, *5*, 8384−8391.
(51) Liu, M. Z.; Guyot-Sionnest, P. *J. Phys. Chem. B* **2005**, *109*, 22192−22200.
(52) Goodman, C. M.; McCusker, C. D.; Yilmaz, T.; Rotello, V. M. *Bioconjugate Chem.* **2004**, *15*, 897−900.
(53) Noh, J.; Jang, S.; Lee, D.; Shin, S.; Ko, Y. J.; Ito, E.; Joo, S. W. *Curr. Appl. Phys.* **2007**, *7*, 605−610.
(54) Alkilany, A. M.; Nagaria, P. K.; Hexel, C. R.; Shaw, T. J.; Murphy, C. J.; Wyatt, M. D. *Small* **2009**, *5*, 701−708.
(55) Zhang, L. M.; Wang, L. M.; Hu, Y. L.; Liu, Z. G.; Tian, Y.; Wu, X. C.; Zhao, Y. L.; Tang, H. R.; Chen, C. Y.; Wang, Y. L. *Biomaterials* **2013**, *34*, 7117−7126.
(56) Barros, L. F.; Kanaseki, T.; Sabirov, R.; Morishima, S.; Castro, J.; Bittner, C. X.; Maeno, E.; Ando-Akatsuka, Y.; Okada, Y. *Cell Death Differ.* **2003**, *10*, 687−697.
(57) Jewell, S.; Bellomo, G.; Thor, H.; Orrenius, S.; Smith, M. *Science* **1982**, *217*, 1257−1259.
(58) Nikoobakht, B.; El-Sayed, M. A. *Langmuir* **2001**, *17*, 6368−6374.
(59) Chanana, M.; Rivera-Gil, P.; Correa-Duarte, M. A.; Liz-Marzan, L. M.; Parak, W. J. *Angew. Chem., Int. Ed.* **2013**, *52*, 4179−4183.
(60) Li, W.; Zhao, L. N.; Wei, T. T.; Zhao, Y. L.; Chen, C. Y. *Biomaterials* **2011**, *32*, 4030−4041.